CHEMISTRY OF MATERIALS
Article

Chem. Mater. **2010,** *22,* 2741–2749 2741
DOI:10.1021/cm903494f

Synthesis and Electrophoretic Deposition of Single-Walled Carbon Nanotube Complexes with a Conjugated Polyelectrolyte

Travis Casagrande,[†] Patigul Imin,[‡] Fuyong Cheng,[‡] Gianluigi A. Botton,[†] Igor Zhitomirsky,[†] and Alex Adronov*[,‡]

[†]*Department of Materials Science and Engineerin,g McMaster University, 1280 Main Street West, Hamilton, Ontario, Canada L8S 4L7,* [‡]*Department of Chemistry, McMaster University, 1280 Main Street West, Hamilton, Ontario, Canada L8S 4M1, and*

Received November 17, 2009. Revised Manuscript Received April 3, 2010

A conjugated tertiary amine-functionalized polymer, poly(9,9-bis(diethylaminopropyl)-2,7-fluorene-co-1,4-phenylene), was synthesized and employed in the supramolecular functionalization of single-walled carbon nanotubes. The formation of stable solutions in organic solvents, as well as in water upon protonation of the amine groups, indicates strong supramolecular interactions between the polymers and the carbon nanotube surface. UV−vis absorption spectroscopy and Raman spectroscopy were utilized to characterize the resulting functionalized nanotubes and it was found that the nanotube structure was unchanged due to the nature of noncovalent functionalization, thus preserving the nanotube's inherent properties. Electrophoretic deposition techniques were developed to create uniform films of this polymer and also a mixture of the polymer with the supramolecularly functionalized carbon nanotubes. The deposition mechanism involves the electrophoresis of the charged polymer species in an acid solution followed by the charge neutralization of the polymer species at the high pH region of the cathode surface. Scanning electron microscopy was used to visualize cross sections of the films as well as the film surfaces, showing uniform coatings that are free of cracks but contain small pores having diameters below 100 nm. The deposition rate was measured using a quartz crystal microbalance and found to vary with voltage and solution concentration. Control over film thickness was demonstrated in the range of approximately 100 nm to 10 μm.

Introduction

Carbon nanotubes (CNTs) have received significant recent attention as a result of their unique mechanical and electronic properties.[1−5] This attention has steadily increased as new methods for incorporating them within nanocomposites and a myriad of devices have been developed.[6] In this context, solution-phase manipulation of CNTs is an area of current interest, as many of the devices and composites require homogeneous mixtures of nanotubes within various host materials.[7] Considering that chemical functionalization of CNTs dramatically improves their solubility in a variety of solvents, significant effort has been invested in the development of functionalization strategies, which include both covalent and supramolecular approaches.[5,8−11] In particular, for applications that depend on electronic conductivity of CNTs, supramolecular functionalization is preferable because this approach does not introduce defects on the nanotube sidewall. Supramolecular functionalization through π-stacking with planar aromatic molecules (i.e., pyrene) has recently become increasingly investigated.[12−16] However, for most small molecules, the π-stacking interaction with nanotube sidewalls is relatively weak, requiring a large excess of the adduct to stabilize nanotubes in solution. The interaction strength between the adsorbate and the CNT surface can be improved by using multivalent binding interactions with polymers, both natural and synthetic.[10] It has been

*Corresponding author. E-mail: adronov@mcmaster.ca. Fax: (905) 521-2773. Phone: (905) 525-9140.

(1) Ajayan, P. M. *Chem. Rev.* **1999**, *99*, 1787.
(2) Terrones, M.; Hsu, W. K.; Kroto, H. W.; Walton, D. R. M. *Top. Curr. Chem.* **1999**, *199*, 189.
(3) Collins, P. G.; Avouris, P. *Sci. Am.* **2000**, *283*, 62.
(4) Baughman, R. H.; Zakhidov, A. A.; De Heer, W. A. *Science* **2002**, *297*, 787.
(5) Tasis, D.; Tagmatarchis, N.; Bianco, A.; Prato, M. *Chem. Rev.* **2006**, *106*, 1105.
(6) Endo, M.; Strano, M. S.; Ajayan, P. M. *Top. Appl. Phys.* **2008**, 13.
(7) Coleman, J. N.; Khan, U.; Blau, W. J.; Gun'ko, Y. K. *Carbon* **2006**, *44*, 1624.
(8) Hirsch, A. *Angew. Chem., Int. Ed.* **2002**, *41*, 1853.
(9) Bahr, J. L.; Tour, J. M. *J. Mater. Chem.* **2002**, *12*, 1952.
(10) Bahun, G. J.; Cheng, F.; Homenick, C. M.; Lawson, G.; Zhu, J.; Adronov, A.The Polymer Chemistry of Carbon Nanotubes. In Chemistry of Carbon Nanotubes; Basiuk, V. A., Basiuk, E. V., Eds.; American Scientific Publishers: Stevenson Ranch, CA, **2008**; Vol. *2*, p 191.
(11) Homenick, C. M.; Lawson, G.; Adronov, A. *Polym. Rev.* **2007**, *47*, 265.
(12) Chen, R. J.; Zhang, Y.; Wang, D.; Dai, H. *J. Am. Chem. Soc.* **2001**, *123*, 3838.
(13) Nakashima, N.; Tomonari, Y.; Murakami, H. *Chem. Lett.* **2002**, 638.
(14) Murakami, H.; Nomura, T.; Nakashima, N. *Chem. Phys. Lett.* **2003**, *378*, 481.
(15) Fernando, K. A. S.; Lin, Y.; Wang, W.; Kumar, S.; Zhou, B.; Xie, S.; Cureton, L. T.; Sun, Y. *J. Am. Chem. Soc.* **2004**, *126*, 10234.
(16) Li, H.; Zhou, B.; Lin, Y.; Gu, L.; Wang, W.; Fernando, K. A. S.; Kumar, S.; Allard, L. F.; Sun, Y. *J. Am. Chem. Soc.* **2004**, *126*, 1014.

Published on Web 04/19/2010

shown that highly stable and concentrated nanotube solutions can be achieved with a variety of conjugated polymers.[17−24] The resulting solutions were shown to contain pristine nanotubes, and allowed manipulation of these structures to produce conducting films on substrates. More recently, it has been shown that conjugated polyelectrolytes can impart a high degree of solubility to single-walled carbon nanotubes (SWNTs) in aqueous solvents, enabling their effective high-resolution patterning on a variety of surfaces.[22] The strong interaction between conjugated polyelectrolytes and SWNTs enables a variety of patterning and deposition methods to be used for assembling SWNTs on surfaces, including the use of electrostatic interactions, layer-by-layer deposition, and electrophoretic deposition on the surface of electrodes. Of these, electrophoretic deposition (EPD) of supramolecularly functionalized SWNTs has received relatively little attention.

EPD is achieved via the motion of charged particles or polymers in a stable suspension toward an electrode under the influence of an electric field, and is an attractive technique for the fabrication of polymer−CNT composite films.[25−27] Bath compositions for EPD can include various additives, which provide stabilization and charging of particles within suspensions.[27−30] Deposit formation can be achieved via coagulation and precipitation of the particles at the electrode surface. The electrostatic repulsion of charged particles has been shown to induce stabilization of the particles in bulk suspensions; however, it impedes deposit formation at the electrodes.[31] This problem can be addressed through the use of polyelectrolytes with pH-dependent charge.[31] Many investigations have been focused on the EPD of cationic polyelectrolytes with amine groups such as chitosan, poly(ethylenimine), poly(allylamine hydrochloride) and poly(vinyl amine).[31,32] Within these examples, the protonation of the polymers' amine groups resulted in solutions of cationic polymers for EPD, which were subsequently deprotonated upon approaching the high pH region at the cathode surface, resulting in the formation of insoluble films.[31,32]

The goal of the present study was to investigate the interaction between an amine-functionalized conjugated polymer and the surface of single-walled carbon nanotubes, where the polymer serves not only to impart solubility to the nanotubes, but also to act as a weak polyelectrolyte that enables electrophoretic deposition on the surface of electrodes. Protonation of the amine groups under slightly acidic conditions provided the charge necessary to impart a high degree of nanotube solubility in polar solvents, such as water and ethanol, through electrosteric stabilization. Under these acidic conditions, deposition of the polymer−nanotube composite onto the surface of various electrodes was found to proceed with excellent control of deposition rate, yield, and film uniformity. Electrophoretically deposited composite films of amine-functionalized conjugated polymers and polymer-functionalized SWNTs could have potential applications in a variety of optoelectronic devices. Recent investigations have shown the successful application of functionalized-SWNT/conjugated-polymer composite films as the active layer in bulk heterojunction type organic solar cell devices.[33−41] This study demonstrates that EPD is an alternative and more versatile method of producing films of polymer/SWNT composites relative to the more common methods such as spin coating, drop casting, spray deposition, or thermal evaporation. EPD should therefore be applicable to the development of future devices that incorporate carbon nanotubes as active components.

Experimental Section

General. Purified grade single-walled carbon nanotubes (SWNTs), produced by the HiPco process, were purchased from Carbon Nanotechnologies, Inc. (Houston, TX). 2,7-dibromo-9,9-bis(3′-bromopropyl)fluorene (**2**) was synthesized according to literature procedures.[42] All other reagents were purchased from commercial suppliers and used as received. NMR spectroscopy was performed on a Bruker 200 MHz instrument, and spectra were referenced to the solvent signal. High-resolution EI-MS measurements were done on the Micromass Ultima Global instrument (quadrupole time-of-flight). Raman spectroscopy was performed on a Renishaw InVia Raman spectrometer equipped with a 25 mW argon ion laser (514 nm), a 300 mW Renishaw 785 nm laser, 1800 L mm^{-1} and 1200 L mm^{-1} gratings for the two lasers, respectively, and a high-resolution mapping stage. The 785 nm laser was operated at 5% intensity to avoid damage to the sample. Atomic Force Microscopy (AFM) was carried out using a Digital Instruments NanoScope IIIa Multimode AFM in tapping mode with standard AFM tips and with

(17) Curran, S. A.; Ajayan, P. M.; Blau, W. J.; Carroll, D. L.; Coleman, J. N.; Dalton, A. B.; Davey, A. P.; Drury, A.; McCarthy, B.; Maier, S.; Strevens, A. *Adv. Mater.* **1998**, *10*, 1091.
(18) Star, A.; Stoddart, J. F.; Steuerman, D.; Diehl, M.; Boukai, A.; Wong, E. W.; Yang, X.; Chung, S.; Choi, H.; Heath, J. R. *Angew. Chem., Int. Ed.* **2001**, *40*, 1721.
(19) Tang, B. Z.; Xu, H. *Macromolecules* **1999**, *32*, 2569.
(20) Chen, J.; Liu, H.; Weimer, W. A.; Halls, M. D.; Waldeck, D. H.; Walker, G. C. *J. Am. Chem. Soc.* **2002**, *124*, 9034.
(21) Rice, N. A.; Soper, K.; Zhou, N.; Merschrod, E.; Zhao, Y. *Chem Commun* **2006**, 4937.
(22) Cheng, F.; Imin, P.; Lazar, S.; Botton, G. A.; De Silveira, G.; Marinov, O.; Deen, J.; Adronov, A. *Macromolecules* **2008**, *41*, 9869.
(23) Cheng, F.; Imin, P.; Maunders, C.; Botton, G.; Adronov, A. *Macromolecules* **2008**, *41*, 2304.
(24) Chen, F.; Wang, B.; Chen, Y.; Li, L. *Nano Lett.* **2007**, *7*, 3013.
(25) Van Tassel, J. J.; Randall, C. A. *J. Mater. Sci.* **2006**, *41*, 8031.
(26) Van, D. B.; Vandeperre, L. J. *Annu. Rev. Mater. Sci.* **1999**, *29*, 327.
(27) Ferrari, B.; Moreno, R. *J. Electrochem. Soc.* **2000**, *147*, 2987.
(28) Besra, L.; Liu, M. *Prog. Mater Sci.* **2007**, *52*, 1.
(29) Wang, Y. H.; Chen, Q. Z.; Cho, J.; Boccaccini, A. R. *Surf. Coat. Technol.* **2007**, *201*, 7645.
(30) Cao, G. *J. Phys. Chem. B* **2004**, *108*, 19921.
(31) Zhitomirsky, I. *J. Mater. Sci.* **2006**, *41*, 8186.
(32) Pang, X.; Casagrande, T.; Zhitomirsky, I. *J. Colloid Interface Sci.* **2009**, *330*, 323.
(33) Kymakis, E.; Amaratunga, G. A. J. *Rev. Adv. Mater. Sci.* **2005**, *10*, 300.
(34) Sgobba, V.; Guldi, D. M. *J. Mater. Chem.* **2008**, *18*, 153.
(35) Yun, D.; Feng, W.; Wu, H.; Li, B.; Liu, X.; Yi, W.; Qiang, J.; Gao, S.; Yan, S. *Synth. Met.* **2008**, *158*, 977.
(36) Arranz-Andres, J.; Blau, W. J. *Carbon* **2008**, *46*, 2067.
(37) Kymakis, E.; Alexandrou, I.; Amaratunga, G. A. J. *J. Appl. Phys.* **2003**, *93*, 1764.
(38) Previti, F.; Patane, S.; Allegrini, M. *Appl. Surf. Sci.* **2009**, *255*, 9877.
(39) Kymakis, E.; Amaratunga, G. A. J. *Appl. Phys. Lett.* **2002**, *80*, 112.
(40) Landi, B. J.; Raffaelle, R. P.; Castro, S. L.; Bailey, S. G. *Prog. Photovoltaics Res. Appl.* **2005**, *13*, 165.
(41) Rud, J. A.; Lovell, L. S.; Senn, J. W.; Qiao, Q.; Mcleskey, J. T., Jr. *J. Mater. Sci.* **2005**, *40*, 1455.
(42) Zhou, G.; Qian, G.; Ma, L.; Cheng, Y.; Xie, Z.; Wang, L.; Jing, X.; Wang, F. *Macromolecules* **2005**, *38*, 5416.

scan rates at or below 0.5 Hz. Ultrasonication was done in a Branson Ultrasonics B1510 bath sonicator. Filtration was done through a 200 nm-pore Teflon membrane (Millipore). The surface microstructures of the deposited coatings as well their cross sections were investigated using a JEOL JSM-7000F scanning electron microscope (SEM). Cross section specimens were prepared by deposition onto a piece of a platinum-coated silicon wafer substrate which was then fractured cleanly along a cleavage plane by pressing at the edge of the wafer using a tungsten carbide scriber, thus exposing the cross section of the film. The SEM specimens were coated with 4−8 nm of platinum using the Gatan Precision Etching Coating System (model 682) to improve surface conductivity and increase electron yield. The thickness of coatings on ITO substrates was measured using a Veeco Wyko NT1100 optical profilometer using VSI mode for coatings thicker than 160 nm, and PSI mode for thinner coatings. Scratches from a razor blade were utilized to create trenches in the coating to allow measurement of the height difference from the substrate surface to the coating surface. The transmittance of coatings on ITO substrates was determined through their absorbance spectrum from 300 to 800 nm, using a Varian Cary 50 Bio UV−visible Spectrophotometer, with a clean ITO covered glass substrate as the baseline. All UV−vis absorption spectra were also measured using the same Varian Cary 50 Bio UV−visible spectrophotometer.

Synthesis of 2,7-Dibromo-9,9-bis[3′-(*N*,*N*-diethylamino)propyl]-fluorene (3). 2,7-dibromo-9,9-bis(3′-bromopropyl)fluorene (**2**)[42] (6.0 g, 10.6 mmol), diethylamine (10 mL, 96.6 mmol), potassium carbonate (10 g, 72.3 mmol), and potassium iodide (1.0 g, 6.0 mmol) were added to acetone (60 mL) in a 100 mL round-bottom flask, equipped with a stir bar and a reflux condenser, under Ar. The reaction was then heated to reflux in the dark and stirred for 16 h. The mixture was filtered through a fritted funnel and the filtrate was evaporated in vacuo. The organic components were dissolved in CH_2Cl_2 (100 mL), washed with water (3 × 100 mL), and dried over anhydrous Na_2SO_4. CH_2Cl_2 solvent was removed in vacuo, and the desired product **3** was obtained as a white solid (5.8 g, 99%). ^{1}H NMR ($CDCl_3$, 200 MHz): δ 7.57−7.45 (m, 6 H), 2.33 (q, 8 H, J = 7.0 Hz), 2.19 (t, 4 H, J = 7.6 Hz), 1.98 (t, 4 H, J = 8.0 Hz), 0.91 (t, 12 H, J = 7.2 Hz), 0.83−0.72 (m, 4H) . ^{13}C NMR ($CDCl_3$, 50 MHz): δ 152.18, 139.16, 130.39, 126.24, 121.65, 121.29, 55.42, 53.13, 46.47, 37.91, 21.72, 11.54. HRMS (EI) m/z calcd for $C_{27}H_{39}Br_2N_2$ $[M]^+$ 549.1480, found 549.1447.

Synthesis of Poly(9,9-bis(diethylaminopropyl)-2,7-fluorene-co-1,4-phenylene) (PDAFP) (4). To a 100 mL flask charged with 40 mL of DMF and Cs_2CO_3 (6.0 g, 18.5 mmol) was added **3** (1.10 g, 2.0 mmol) and 1,4-benzenediboronic acid bis(pinacol)ester (0.66 g, 2.0 mmol). The mixture was then bubbled with N_2 for 15 min, degassed via four freeze−pump−thaw cycles, and finally backfilled with Ar. A catalytic amount $Pd(PPh_3)_4$ (1.0 mol %) was added, and the resulting mixture was stirred at 100 °C under Ar overnight. After being cooled to room temperature, the solution was precipitated via dropwise addition to 1 L of water and filtered. The residue was washed with water, (4 × 250 mL) and methanol (50 mL). After being dried under a vacuum for 20 h, a white powder was obtained (0.85 g, 90%). ^{1}H NMR ($CDCl_3$, 200 MHz): δ 7.82 (br, 10 H), 2.36 (br, 16 H), 0.92 (br, 16 H). UV−vis (EtOH/H_2O, 2:1, plus 0.2% acetic acid): λ_{max} = 373 nm.

Preparation of Polymer Solutions for EPD. To a mixture of PDAFP powder in water (polymer concentration of 6 g L^{-1}), acetic acid was slowly added up to a concentration of 0.2 vol % while continuously stirring. This stock polymer solution was diluted with ethanol and water to the various concentrations used for EPD experimentation, typically 0.25 g L^{-1} in 95/5 ethanol/water.

Preparation of Polymer-Functionalized Carbon Nanotube Solutions for EPD. SWNTs were dispersed in absolute ethanol using ultrasonication for 20 min. The water-soluble polymer stock solution was added to the nanotube dispersion until the concentration of polymer was 2 g L^{-1}, the concentration of SWNTs was 5% of the polymer weight, and the solvent ratio was 2:1 ethanol:water. The mixture was ultrasonicated for 1 h, resulting in the PDAFP functionalization of exfoliated individual SWNTs. The PDAFP-SWNT solution was then centrifuged for 30 min at 2576 g and left to settle for 2 days. The undisturbed solution was then extracted with a pipet, whereas any remaining solid material was left behind at the bottom of the centrifuge tubes. This 2 g L^{-1} solution of functionalized nanotubes and free polymer was then diluted to the various concentrations used for EPD experimentation, typically 0.25 g L^{-1} in 95/5 ethanol/water.

Electrophoretic Deposition (EPD). EPD of either polymer films or composite polymer-SWNT films was performed from solutions prepared as detailed above. Cathodic deposits were obtained on stainless steel, ITO-coated glass, platinized silicon wafer, and gold coated quartz crystal (Seiko) substrates. The platinized silicon wafer contained a Pt conducting electrode layer (1500 Å) and a Ti adhesion layer (300 Å), prepared by sputtering. The substrate area was varied in the range of 0.2−12 cm^2. Platinum foil was used as an anode. The deposition process was investigated at different voltages in the range of 30−80 V and the distance between the electrodes was 14 mm.

Quartz Crystal Microbalance Studies of the Deposition Yield. The deposition process has been investigated using a quartz crystal microbalance QCM 922 (Princeton Applied Research) controlled by the WinEchem software. The deposit mass Δm was calculated using Sauerbrey's equation:

$$-\Delta F = \frac{2F_0^2}{A\sqrt{\rho_q \mu_q}}\Delta m \quad (1)$$

where ΔF is measured frequency decrease of quartz crystal oscillations, F_0 is the parent resonant frequency of the quartz crystal (9 MHz), A is the electrode area (0.2 cm^2), ρ_q is the density of the quartz, and μ_q is the shear modulus of quartz. QCM measurements were carried out using voltages in the range of 3−5 V and with a 3 mm separation distance between the electrodes. To avoid problems that occur in the mass gain measurement when the viscosity is too high, low polymer solution concentrations in the range of 0.05−0.1 g L^{-1} were used.

Results and Discussion

The synthesis of the tertiary amine-functionalized poly-(9,9-bis(diethylaminopropyl)-2,7-fluorene-co-1,4-phenylene) (PDAFP) polymer **4** is depicted in Scheme 1. Briefly, this polymer was prepared by treating commercially available 2,7-dibromofluorene with 1,3-dibromopropane in the presence of NaOH to yield 2,7-dibromo-9,9-bis(3′-bromopropyl)fluorene (**2**), as described previously.[42] Subsequent treatment of **2** with diethylamine afforded the amine-functionalized fluorene monomer **3** in near quantitative yield. Polymerization of monomer **3** with commercially available 1,4-benzenediboronic acid bis(pinacol)ester using Suzuki polycondensation conditions produced PDAFP (**4**) in 90% yield. The structure of polymer **4** was verified only by ^{1}H NMR and UV−vis spectroscopy, as molecular weight

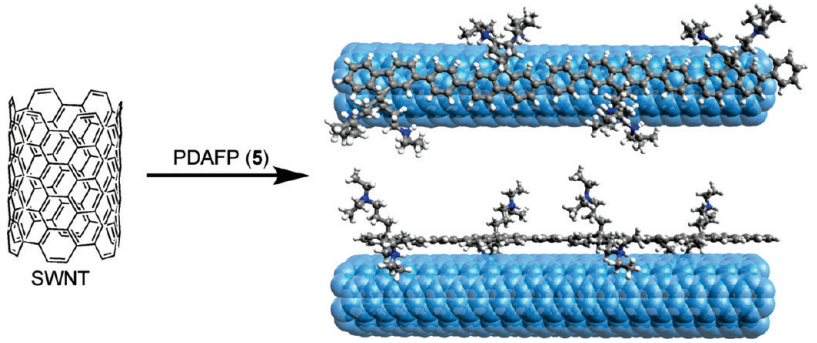

Figure 1. Schematic representation of the supramolecular interaction between protonated PDAFP (**5**) and SWNTs, showing a top and side view on the upper and lower right, respectively. Energy-minimized structures were obtained using Avogadro (ver. 0.9.5) and the Universal Force Field (UFF, molecular mechanics) provided with this software package.

Scheme 1

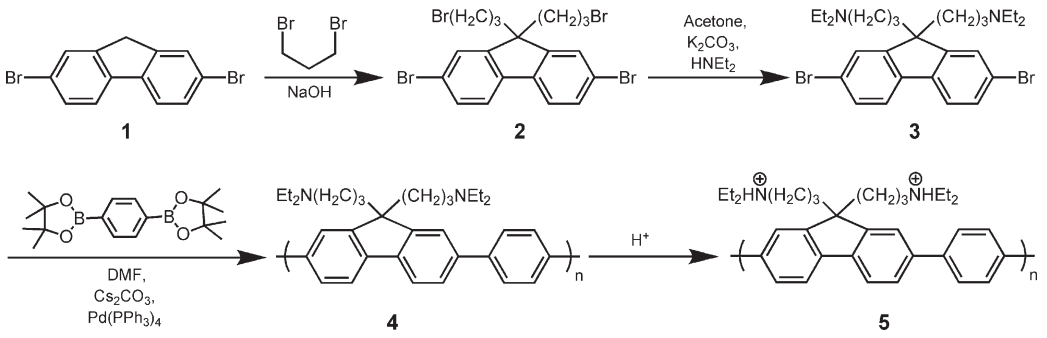

data could not be obtained by conventional size exclusion chromatography (SEC) because of the irreversible adsorption of the polymer onto the SEC column packing material. All attempted SEC experiments resulted in no signal in the elution volume, with a corresponding increase in backpressure on the SEC instrument. We therefore could only estimate the molecular weight by comparing the UV−vis absorption maximum (in $CHCl_3$) to analogous previously reported polymers.[43,44] On the basis of this comparison, we estimate that the molecular weight of polymer **4** is in the range of 8000 g mol^{-1}.

The neutral polymer **4** was found to be soluble in various organic solvents, including DMF, chloroform, and THF. Based on previous work on the interactions of conjugated polymers with SWNTs,[22−24] it was not surprising that mixture and brief sonication of **4** with SWNTs in THF produced dark, stable, homogeneous suspensions of SWNTs. From these results, it is clear that sonication breaks up large nanotube bundles and allows the conjugated polymer backbone to π-stack to the nanotube surface, thereby stabilizing it in solution. However, the neutral complex between polymer **4** and SWNTs was not applicable to electrophoretic deposition (EPD), as it is necessary to produce charged species in solution for EPD to be successful.

Although polymer **4** was found to be completely insoluble in water and low-boiling alcohols (methanol and ethanol) under neutral conditions, addition of small amounts of acetic acid (0.2% vol/vol) to these solvents resulted in complete and rapid dissolution of the polymer, because of partial protonation of the amine side chains. The excellent solubility of the polymer in acidified solution led us to investigate the formation of polymer−nanotube complexes in these acidic media. Specifically, we focused on investigation of acidified ethanol/water mixtures, which were prepared by dilution of a concentrated aqueous solution of polymer (6 g L^{-1} containing 0.2 vol % of acetic acid) with ethanol to obtain the desired solvent ratio (95/5 ethanol/water, vol/vol). The high ethanol content in these mixtures was important in preventing gas evolution from electrolysis of water at the cathode, which degrades film quality. It was found that addition of SWNTs in these acidified ethanol/water solutions of **4** resulted in the formation of concentrated, homogeneous solutions of polymer-functionalized SWNTs after sonication, depicted schematically in Figure 1. It should be noted that filtration and extensive washing of the polymer-functionalized SWNTs was performed to remove excess free polymer from solution, which was easily detectable because of its strong fluorescence in solution. After complete removal of the excess polymer, the remaining material retained its solubility in the acidified 95/5 ethanol/water mixtures, attesting to the fact that the polymer−nanotube interaction is extremely strong.

The supramolecular interaction of PDAFP with SWNTs in the acidified ethanol/water solutions was investigated by UV−vis absorption spectroscopy. Figure 2 depicts the spectra of the polymer, SWNTs, and the polymer−SWNT complex in the acidified solution. The polymer absorption is

(43) Huang, F.; Wu, H.; Wang, D.; Yang, W.; Cao, Y. *Chem. Mater.* **2004**, *16*, 708.
(44) Nag, O. K.; Kang, M.; Hwang, S.; Suh, H.; Woo, H. Y. *J. Phys. Chem. B* **2009**, *113*, 5788.

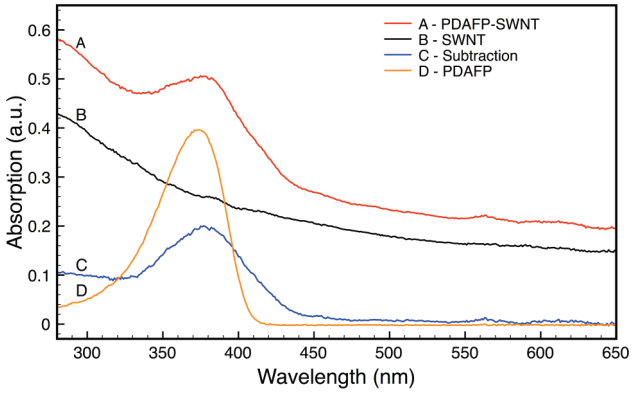

Figure 2. UV−vis absorption data for the (A) PDAFP-SWNT complex, (B) SWNTs, (D) free PDAFP polymer, and (C) the polymer contribution to the polymer−nanotube complex spectrum. The spectrum of the PDAFP-SWNT and free PDAFP samples were acquired in acidified ethanol/water (95/5 vol/vol) solutions, whereas the SWNT spectrum was obtained from an aqueous dispersion with 1 wt % sodium dodecyl sulfate serving as a surfactant.

visible within the spectrum of the polymer−nanotube complex as a broad peak centered around 380 nm, clearly indicating its presence in significant quantity even though excess polymer in solution has been removed by filtration and washing. In addition, subtraction of the normalized SWNT absorption spectrum from that of the polymer-SWNT complex resulted in a spectrum that corresponds to just the polymer contribution to the polymer−SWNT complex absorption (labeled "subtraction" in Figure 2). Comparison of the subtraction spectrum to the absorption of free polymer revealed a characteristic bathochromic shift in the polymer absorption, which occurs upon nanotube complexation.[23] This shift may be attributed to an increase in the effective conjugation length of the polymer, caused by adoption of a more planar structure of its backbone upon interaction with the SWNT surface.[23] Alternatively, this shift may be directly caused by the π-stacking interaction with the nanotube sidewall, which leads to delocalization of π electrons onto the SWNT surface and stabilization of the polymer excited state.

Raman spectroscopy of the polymer-functionalized SWNTs, using 785 nm excitation, indicated that practically no structural changes had occurred as a result of the supramolecular interaction with polymer **4**. All of the characteristic Raman-active stretching vibrations, including the graphitic (G) band at ~1590 cm^{-1}, the disorder (D) band at ~1300 cm^{-1}, and the radial breathing modes (RBM) in the range of 150−300 cm^{-1}, are observable and comparable to those of pristine SWNTs (Figure 3i, curves A and B). Specifically, the unchanged nature of the D band indicates that interaction with the polymer does not lead to any structural changes or defects within the nanotube sidewalls. Upon closer examination of the RBM signals, small shifts and changes in intensity of several signals can be observed, indicating that different surface functionalization causes different tube chiralities and diameters to come in resonance with the frequency of the incident laser. It is therefore difficult to attribute the changes in RBM peak intensity and frequency to any diameter selectivity by the polymer. However, the signal at ~265 cm^{-1} has recently

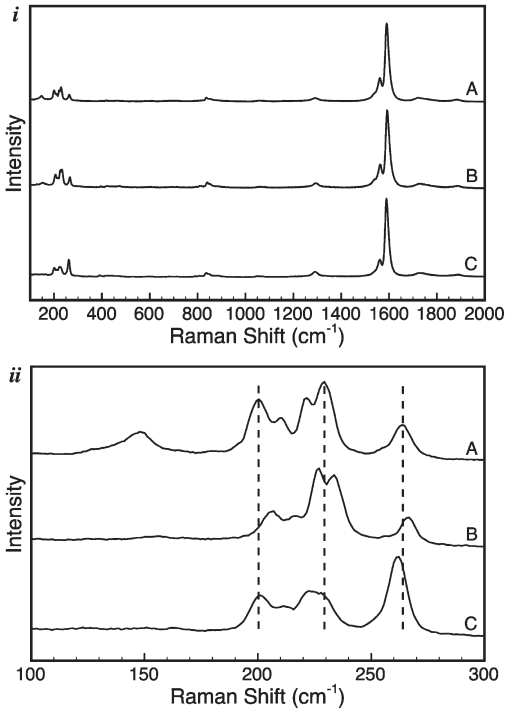

Figure 3. (i) Raman spectra of (A) pristine SWNTs, (B) polymer-functionalized SWNTs, and (C) an electrophoretically deposited film containing SWNTs, all normalized to the graphitic band at ~1590 cm^{-1}. (ii) Close-up of the radial breathing mode signals of (A) pristine SWNTs, (B) polymer-functionalized SWNTs, and (C) an electrophoretically deposited film containing SWNTs, normalized to the peak of maximum intensity. Dotted lines are provided to guide the eye. All spectra were obtained with 785 nm excitation.

been found to correlate with the presence of nanotube bundles within a sample.[45] Comparison of the relative peak maxima of the signals at ~265 and ~230 cm^{-1} in curves A and B (Figure 3ii) revealed that a slight decrease in the signal at 265 cm^{-1} occurs upon supramolecular interaction with PDAFP after drying (the sample preparation involved placing a drop of the polymer−nanotube solution onto a glass microscope slide and allowing it to evaporate). From these data, it seems that the extent of aggregation is decreased when the solution is subjected to the above treatment, versus the original pristine nanotube sample. Upon electrophoretic deposition (vide infra) of the sample onto an electrode, the relative intensity of the signal at ~265 cm^{-1} dramatically increases, indicating that significant aggregation of the nanotubes may be occurring on the electrode surface.

Additional characterization of polymer functionalized carbon nanotubes was performed using atomic force microscopy (AFM). The specimen was prepared by spin coating a dilute solution of functionalized nanotubes onto a freshly cleaved mica substrate. The observation of dispersed individual nanotubes on the substrate surface, shown by AFM analysis in Figure 4, indicates that the separation of large nanotube bundles into individual functionalized carbon nanotubes occurred using PDAFP. Functionalized nanotube diameters

(45) Heller, D. A.; Barone, P. W.; Swanson, J. P.; Mayrhofer, R. M.; Strano, M. S. *J. Phys. Chem. B* **2004**, *108*, 6905.

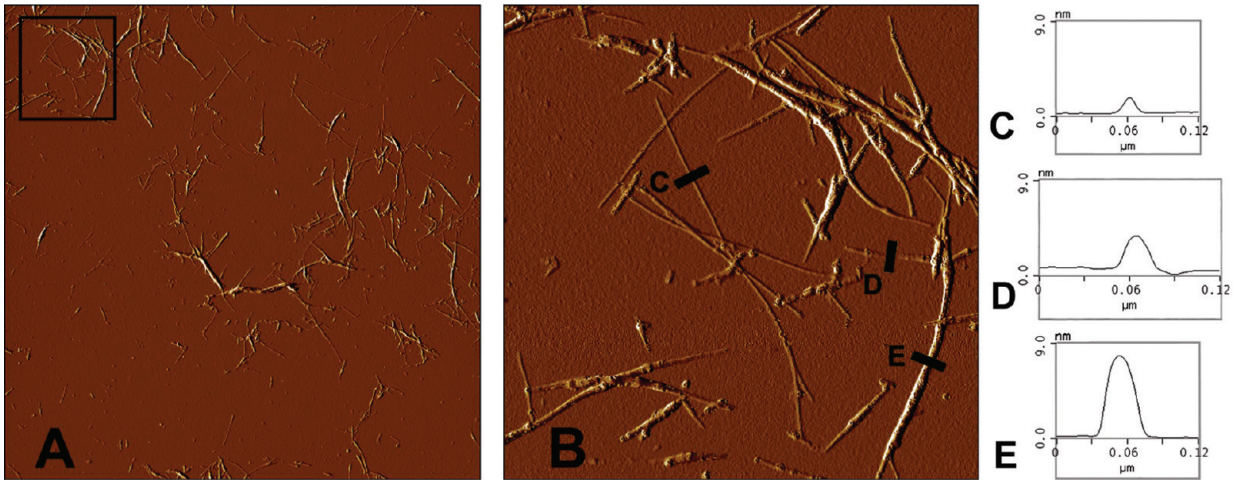

Figure 4. AFM data showing polymer-functionalized carbon nanotubes that have been spin-coated from aqueous solution onto a silicon substrate. (A) 10 μm × 10 μm scan of the sample. (B) The area within the black box in A, showing a higher-magnification 2 μm × 2 μm scan. Averaged section analysis across three different nanotubes in B, depicted by black lines, gave the linear surface profiles C−E, showing that the combined diameter of the nanotubes and the attached polymer ranged from 1.4 to 7.5 nm.

were measured by averaged section analyses across linear regions of various nanotube features (regions shown as black lines in Figure 4 B), producing plots of the average height along the lines (Figure 4C−E). These plots show the combined height of the nanotube and the adsorbed polymer, which ranged from 1.4 to 7.5 nm. These data are consistent with the results of Raman spectroscopy, showing the exfoliation of nanotube bundles into individual nanotubes via polymer functionalization.

Electrophoretic deposition (EPD) studies were initially conducted with PDAFP alone, in order to optimize deposition conditions. These studies were carried out by using a quartz crystal as the cathodic substrate, such that the deposition yield as a function of voltage, polymer concentration, and time could be measured using a quartz crystal microbalance (QCM). Figure 5 depicts a schematic diagram of the experimental setup used in QCM studies of EPD.

In these studies, the EPD process of PDAFP was facilitated by protonation of the polymer under acidic conditions, according to eq 2. At low pH, the protonated polymer behaved as a cationic polyelectrolyte, and, upon applied voltage, migrated to the surface of the cathode. We postulate that, in the vicinity of the cathode, the reduction of water results in the production of hydroxide ions, according to eq 3. This process results in an increased pH at the cathode surface, which neutralizes the polymer that has migrated to the cathode surface as a result of electrophoretic motion (eq 4). The neutralized polymer essentially precipitates onto the surface of the electrode, producing an insoluble, highly uniform deposit. Figure 6 shows three plots of deposition yield versus deposition time measured using the QCM. From these experiments, it is clear that the deposited mass increases with increasing deposition time. In addition, the increase in deposition voltage and/or polymer concentration resulted in an increased deposition yield. These results indicated that the amount

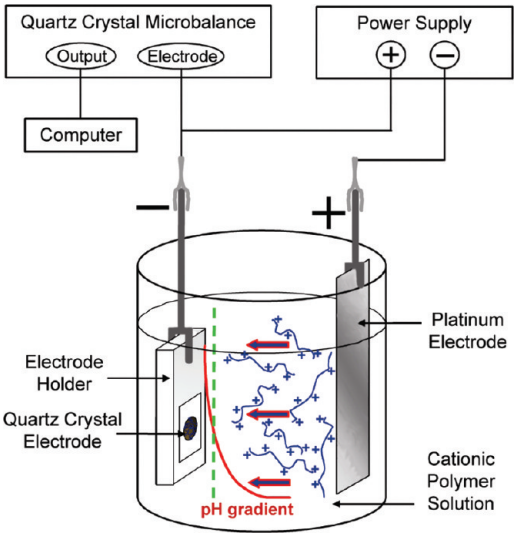

Figure 5. Schematic setup of the QCM study of the EPD of polymer.

of PDAFP deposited on the cathode could be precisely controlled.

$$\text{PDAFP-NEt}_2 + \text{H}_3\text{O}^+ \rightarrow \text{PDAFP-N}^+\text{HEt}_2 + \text{H}_2\text{O} \quad (2)$$

$$2\text{H}_2\text{O} + 2\text{e}^- \rightarrow \text{H}_2 + 2\text{OH}^- \quad (3)$$

$$\text{PDAFP-N}^+\text{HEt}_2 + \text{OH}^- \rightarrow \text{PDAFP-NEt}_2 + \text{H}_2\text{O} \quad (4)$$

To corroborate the QCM studies, we used scanning electron microscopy (SEM) to visualize cross sections of the deposited films. These studies showed that film thickness can be varied in the range of 0−10 μm by variation of polymer concentration, deposition time and voltage. Figure 7 shows typical SEM images of cross sections of the films deposited from 0.25 to 0.5 g L^{-1}

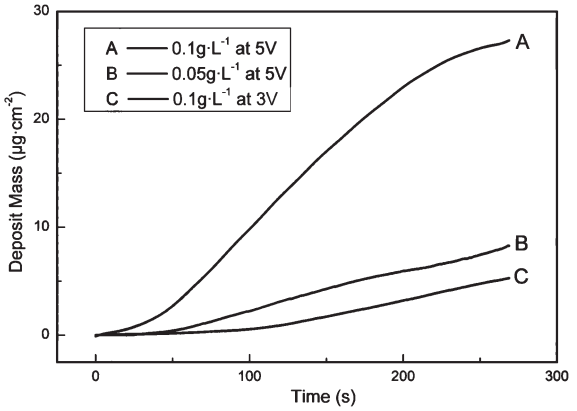

Figure 6. Deposit mass of a polymer film measured using QCM versus the deposition time at different applied voltages and polymer solution concentrations.

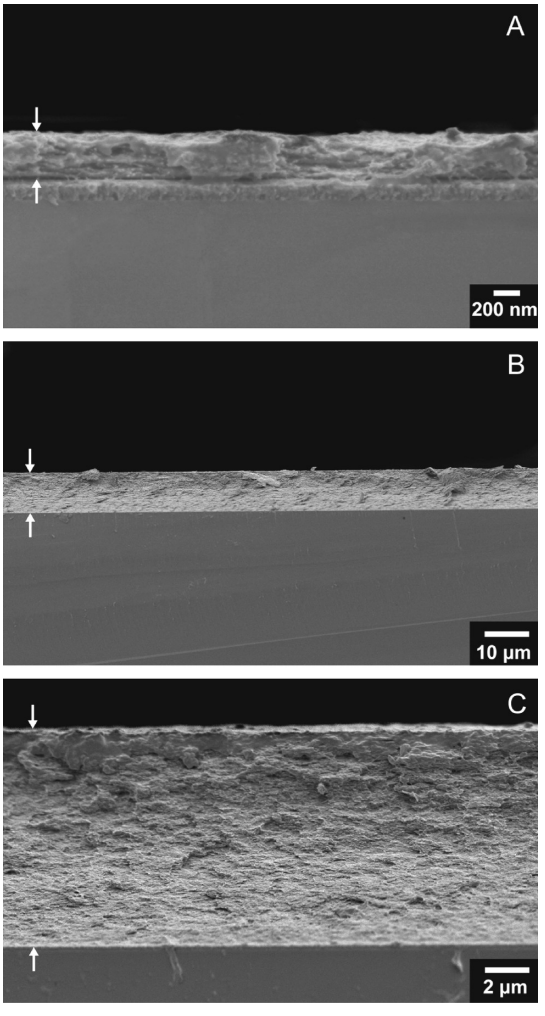

Figure 7. SEM images of cross-sections of polymer films on platinized silicon wafers showing (A) a thin 340 nm film, and (B, C) a thicker 9.6 μm film at different magnifications, deposited at (A) a deposition voltage of 30 V from a 0.25 g L^{-1} polymer solution for 1 min, and (B, C) a deposition voltage of 50 V from a 0.50 g L^{-1} polymer solution for 15 min. Arrows indicate the top and bottom edges of the films.

polymer solutions at deposition voltages of 30−50 V on platinized silicon wafers at different deposition durations. The SEM images show the formation of relatively uniform films of different thickness (Figure 7 A, B). The

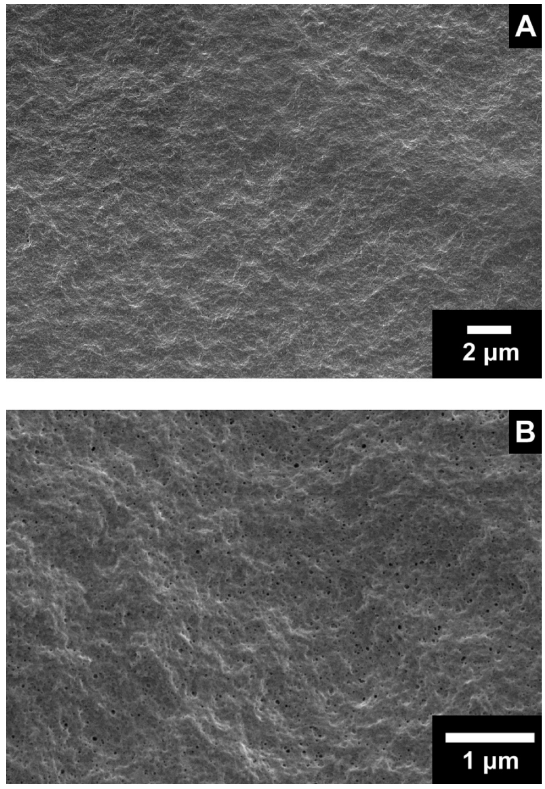

Figure 8. SEM images of a polymer film surface at different magnifications. The film was prepared at a deposition voltage of 50 V from 0.25 g L^{-1} polymer solutions.

SEM image at higher magnification (Figure 7 C) indicates that the films are uniform and exhibit a low degree of porosity. In addition to film cross-sections, film surfaces were also imaged at different magnifications (Figure 8). The image of the film surface at low magnification (Figure 8A) shows that the films were free of cracks and macroscopic voids. However, at higher magnification, small pores having a pore diameter below 50 nm could be observed. Such porosity is attributed to gas evolution during EPD.

The successful electrophoretic deposition of uniform, high-quality PDAFP films allowed for further investigation of composite film deposition, where SWNTs were incorporated in the polymer matrix. As described above, a strong interaction between the PDAFP and the nanotube surface was observed, especially in acidified aqueous solutions where the polymer is protonated. Therefore, composite films containing 5 wt % SWNTs in a PDAFP matrix were deposited from 0.1 to 0.5 g L^{-1} polymer solutions. Figure 9 shows SEM images of the typical cross-sections of composite films of different thickness.

The film thickness was varied in the range of 0.1−10 μm by variation of the deposition time in the range of 1−10 min, and deposition voltage in the range of 30−60 V. The high magnification SEM image (Figure 9C) clearly shows SWNTs within the polymer matrix. Interestingly, a large proportion of SWNTs were observed to be aligned perpendicular to the substrate surface. The alignment of carbon nanotubes perpendicular to the substrate during

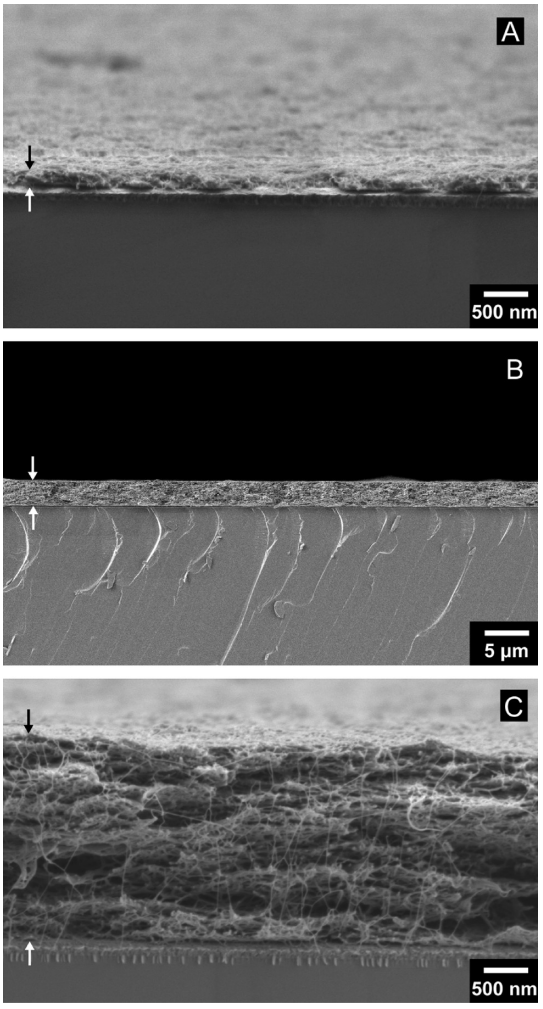

Figure 9. SEM images of cross-sections of polymer-SWNT films on platinized silicon wafers showing (A) a thin 210 nm film, and (B,C) thicker 2.8 μm film at different magnifications. The films were deposited at a deposition voltage of 50 V from 0.1 g L^{-1} polymer solution, containing 5 wt % SWNTs. Arrows indicate the top and bottom edges of the films.

EPD has previously been observed in other investigations.[46−48] The electrophoresis of SWNTs, which have a high aspect ratio, can be described by the equations derived for infinitely long cylindrical colloidal particles[49]

$$\mu_{\perp} = \varepsilon_r \varepsilon_0 \zeta / 2\eta \quad (5)$$

$$\mu_{||} = \varepsilon_r \varepsilon_0 \zeta / \eta \quad (6)$$

where $\mu_{\perp}$ and $\mu_{||}$ are electrophoretic mobilities in transverse and tangential fields, respectively, ε_r is relative permittivity of the medium, ε_0 is the permittivity of vacuum, ζ is zeta potential, and η is viscosity. Equations 5 and 6 indicate that $\mu_{||} > \mu_{\perp}$. Therefore, a higher deposition rate of SWNTs aligned parallel to the electric field can be expected. Moreover, these results suggest that the electric field can provide rotation and preferred alignment of the SWNTs in solution.

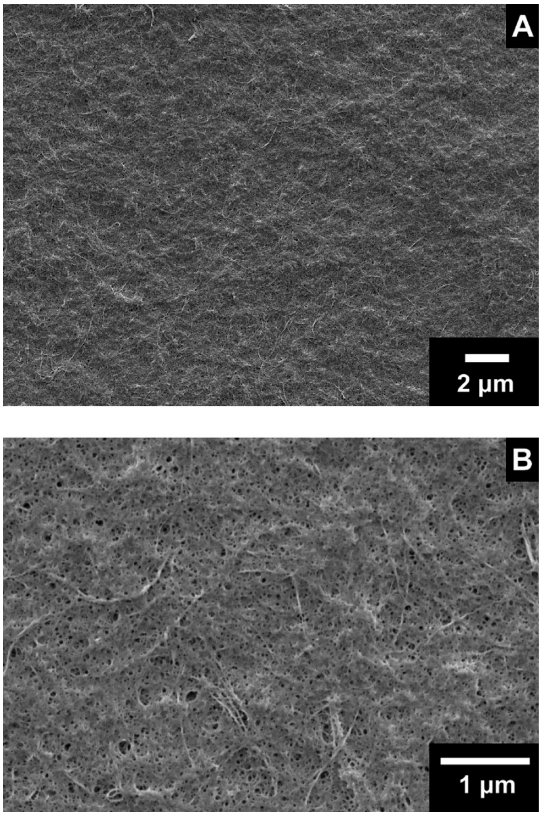

Figure 10. SEM images of a polymer−nanotube film surface at different magnifications. The film was deposited at a deposition voltage of 60 V from 0.25 g L^{-1} polymer solution, containing 5% SWNTs with respect to the polymer mass.

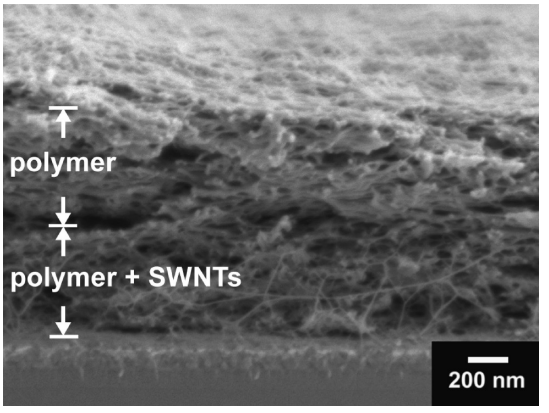

Figure 11. SEM cross-section image of a bilayered EPD film on platinized silicon wafer, with a polymer−SWNT bottom layer and pure polymer top layer.

SEM investigations of the film surfaces at low magnifications again showed that films were crack-free (Figure 10). However, SEM images taken at higher magnification (Figure 10B) showed significant porosity, with pore sizes of variable diameter but typically below 100 nm. The porosity of the films containing SWNTs (Figure 10B) was higher than that of pure polymer films (Figure 8B), presumably resulting from imperfect packing of SWNTs.

In addition to the formation of single-component thin films, EPD enables the fabrication of layered composite

(46) Grandfield, K.; Sun, F.; FitzPatrick, M.; Cheong, M.; Zhitomirsky, I. *Surf. Coat. Technol.* **2009**, *203*, 1481.
(47) Yamamoto, K.; Akita, S.; Nakayama, Y. *Jpn. J. Appl. Phys., Part 2* **1996**, *35*, L917.
(48) Quale, S. L.; Talbot, J. B. *J. Electrochem. Soc.* **2007**, *154*, K25.
(49) Ohshima, H. *J. Colloid Interface Sci.* **2002**, *255*, 202.

Figure 12. Photograph of polymer−SWNT films deposited on ITO-coated glass substrates and placed on top of printed numbers to help visualize the film transparency. The specimen in the #0 position is uncoated. The corners of each square are uncoated because they were covered by electrical contacts to the conducting surface.

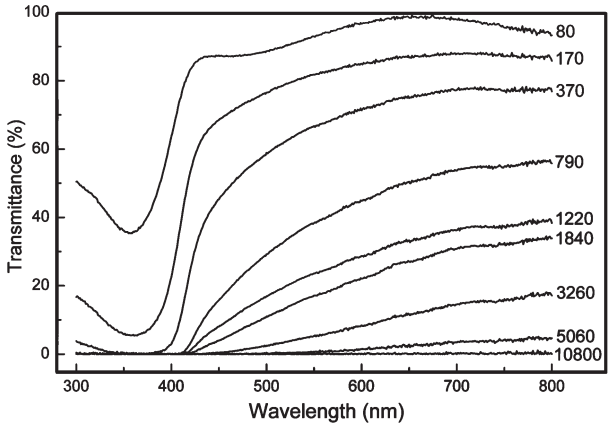

Figure 13. Plot of the transmittance as a function of incident wavelength for each polymer-nanotube coating of different thickness, where the top curve is the thinnest and the bottom curve is the thickest coating. Thickness is given to the right of each curve, measured in nanometers using optical profilometry.

materials containing alternating layers of pure polymer and polymer−SWNT composites. This was easily accomplished by sequentially carrying out the EPD experiment in two different solutions, one containing the polymer−SWNT solution, and the other containing just the polymer. As an example, Figure 11 shows an SEM image of the cross-section of a bilayer film containing a polymer−SWNT bottom layer and a pure polymer top layer. The presence of carbon nanotubes exclusively in the bottom layer can be clearly seen from this image. Therefore, the EPD method is suitable for the fabrication multilayer films, and should similarly be amenable to the preparation of films having a graded composition.

The pure polymer and polymer−SWNT films were also deposited on ITO substrates. Figure 12 shows optical images of the polymer−SWNT composite films of different thickness. This series of films demonstrated control over a broad range of thickness and transparency, with thicknesses of 80, 170, 370, 790, 1220, 1840, 3260, 5060, and 10 800 nm for films 1−9, respectively. The corresponding transmittance data for the films are shown in Figure 13. The absorption peak in the 300−400 nm range is where the polymer strongly absorbs, and the nanotubes contribute broad baseline absorption. The results shown in Figures 12 and 13 indicated that transmittance decreased with increasing film thickness.

Conclusion

The conjugated polymer PDAFP was synthesized and utilized for the supramolecular functionalization of single-walled carbon nanotubes to create stable suspensions in organic and aqueous solvents following acid protonation of the amine side chains. Raman spectroscopy showed that the SWNT structure was preserved after functionalization due to the noncovalent $\pi-\pi$ supramolecular interactions, which is important for maintaining the electrical properties of the carbon nanotubes. Electrophoretic deposition was found to be a successful technique to coat electrodes with films of PDAFP and SWNTs functionalized with PDAFP, using ethanol/water solutions. The deposition mechanism was described as the neutralization of the electrophoretically driven positively charged polymer in the vicinity of the cathode because of the localized increase in pH caused by the generation of hydroxide ions. Quartz crystal microbalance data demonstrated control over the deposition rate and deposited amount by varying the voltage, polymer concentration, and deposition time. Control over film thickness was demonstrated by SEM cross sectional images and by optical profilometry measurements of films ranging in thickness from less than 100 nm to greater than 10 μm. These results demonstrate the viability of utilizing electrophoretic deposition to create uniform coatings of conjugated polymers containing carbon nanotubes with controllable thickness.

Acknowledgment. Financial support for this work was provided by the Natural Sciences and Engineering Research Council of Canada (NSERC), Canada Foundation for Innovation (CFI), and Ontario Innovation Trust (OIT).